



HAL
open science

Seasonal studies of aquatic humic substances from Amazon rivers: characterization and interaction with Cu (II), Fe (II), and Al (III) using EEM-PARAFAC and 2D FTIR correlation analyses

Isabela Carreira Constantino, Lucas Raimundo Bento, Vinicius Sarracini Santos, Leila Soares da Silva, Amanda Maria Tadini, Stéphane Mounier, Alessandro Piccolo, Riccardo Spaccini, Marinônio Lopes Cornélio, Fabiana Maria Monteiro Paschoal, et al.

► To cite this version:

Isabela Carreira Constantino, Lucas Raimundo Bento, Vinicius Sarracini Santos, Leila Soares da Silva, Amanda Maria Tadini, et al.. Seasonal studies of aquatic humic substances from Amazon rivers: characterization and interaction with Cu (II), Fe (II), and Al (III) using EEM-PARAFAC and 2D FTIR correlation analyses. *Environmental Monitoring and Assessment*, 2024, 196 (7), pp.595. 10.1007/s10661-024-12729-5 . hal-04614145

HAL Id: hal-04614145

<https://hal.science/hal-04614145>

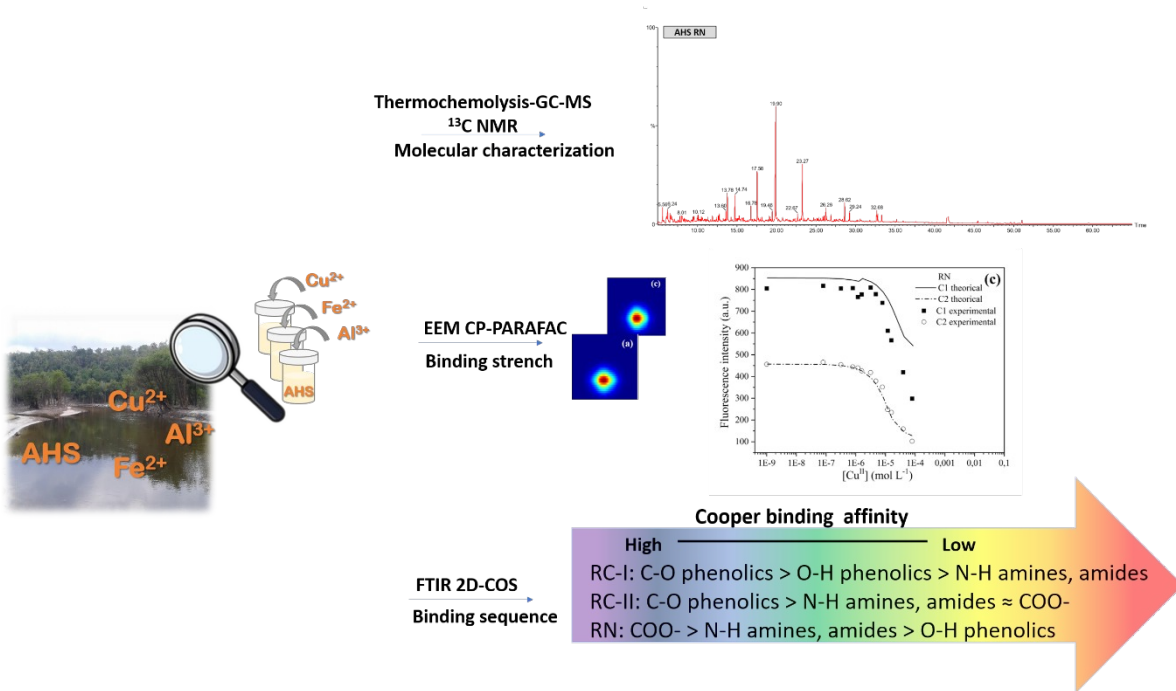
Submitted on 17 Jun 2024

HAL is a multi-disciplinary open access archive for the deposit and dissemination of scientific research documents, whether they are published or not. The documents may come from teaching and research institutions in France or abroad, or from public or private research centers.

L'archive ouverte pluridisciplinaire **HAL**, est destinée au dépôt et à la diffusion de documents scientifiques de niveau recherche, publiés ou non, émanant des établissements d'enseignement et de recherche français ou étrangers, des laboratoires publics ou privés.

41
42
43
44
45
46
47
48
49

Graphical Abstract



50
51
52
53
54
55
56
57
3
4

58

59

60

61

62

63

Abstract

64 Aquatic humic substances (AHS) are defined as important components of organic matter, being
65 composed as small molecules in a supramolecular structure and can interact with metallic ions,
66 thereby altering the bioavailability of these species. To better understand this behavior, AHS were
67 extracted and characterized from Negro rive, located near Manaus city and Carú river, that is
68 situated in Itacoatiara city, an area experiencing increasing anthropogenic actions, both were
69 characterized as blackwater rivers. The AHS were characterized by ¹³C Nuclear Magnetic
70 Ressonance and Thermochemolysis GC-MS to obtain structural characteristics. Interaction studies
71 with Cu (II), Al (III), and Fe (III) were investigated using fluorescence spectroscopy applied to
72 Parallel Factor Analysis (PARAFAC) and Two-Dimensional Correlation Spectroscopy with Fourier
73 Transform Infrared Spectroscopy (2D-COS FTIR). The AHS from dry season had more aromatic
74 fractions not derived from lignin and had higher content of alkyls moities from microbial sources
75 and vegetal tissues of autochthonous origin, while AHS isolated in the rainy season showed more
76 metals in its molecular architecture, lignin units, and polysacharide structures. The study showed
77 that AHS composition from rainy season were able to interact with Al (III), Fe (III) and Cu (II).
78 Two fluorescent components were identified as responsible for interaction: C1(blue-shifted) and C2
79 (red-shifted). C1 showed higher complexation capacities but with lower complexation stability
80 constants (K_{ML} ranged from $0.3-7.9 \times 10^5$) than C2 (K_{ML} ranged from $3.1-10.0 \times 10^5$). 2D-COS FTIR
81 showed that the COO^- and C-O in phenolic were the most important functional groups for
82 interaction with studied metallic ions.

83

5

6

84 **Keywords:** Aquatic humic substances, Complexation, Amazonian, FTIR two-dimension correlation
85 spectroscopy, ¹³C Nuclear Magnetic Resonance.

86

87

88

89

90 **Introduction**

91

92 In aquatic environments, organic matter (OM) formed by the decomposition of plant tissues,
93 animals, microbiological activity, and photochemical processes can originate from both
94 autochthonous sources (derived from microorganisms' byproducts or aquatic organisms) and
95 allochthonous sources (associated with runoff from the soil to aquatic bodies through surface
96 runoff) (Brailsford et al., 2019; Catalán et al., 2013; Uyguner-Demirel & Bekbolet, 2011;
97 Westerhoff et al., 2007). An important fraction of OM is composed of small molecules in a
98 supramolecular structure interaction, such as Van der Waals and hydrogen bonds, among others,
99 being denominated Aquatic humic substances (AHS) (Drosos et al., 2018; Nebbioso & Piccolo,
100 2011; Piccolo, 2002).

101 These AHS can interact with various types of substances, including organic compounds and
102 metallic ions, influencing the bioavailability, distribution, and consequently the toxicity of these
103 compounds in the environment (Y. P. Lee et al., 2023; Leenheer & Croué, 2003; Melo et al., 2012;
104 Muller et al., 2024; Nebbioso & Piccolo, 2013). The interaction between AHS and metallic ions is
105 complex and depends on various factors, such as physicochemical parameters (pH, ionic strength),
106 metallic ions, and AHS features (Boguta et al., 2016; Garnier et al., 2004). Typically, these
107 interactions exhibit a high affinity with metal ions due to the presence of reactive groups, such as
108 carboxylic and phenolic moieties (Y. K. Lee et al., 2021).

109 The Amazon region is a biome of global importance in terms of scale and biodiversity. It
110 boasts the largest watershed in the world, featuring substantial rivers and numerous flood areas that
111 contribute significant amounts of organic matter and metallic species to the aquatic ecosystem.
112 (Jardim et al., 2010). The Amazonian rivers are primarily classified into two types of water:
113 whitewaters, which have near-neutral pH, low dissolved organic matter (DOC), and significant

9

10

114 amounts of particulates; and blackwaters, characterized by a dark-brown color, an acidic pH, and
115 higher DOC levels. (Coimbra Horbe et al., 2013; Constantino et al., 2019; Junk et al., 2015).

116 In accordance with the rainy and dry seasons, the Amazonian rivers undergo changes. The
117 rainy season leads to a threefold increase in the flooded areas of the basin, resulting in elevated
118 content of Aquatic Humic Substances (AHS) with fresh and labile organic matter (OM). Copper,
119 iron, and aluminum are major metals found in the Amazonian rivers of this study area, present
120 during both the dry and rainy seasons. These metals are likely sourced from natural sources in the
121 region. (Constantino et al., 2019). Copper can be derived of weathering and leaching processes, as
122 well as anthropogenic, with its use associated as a fungicide in the region's agricultural activities.
123 The primary sources of iron and aluminum in the aquatic body are from the soil, influenced by the
124 mineralogical composition in the Amazonian region (Tadini et al., 2019). Previous studies on the
125 concentration of these metallic ions found Cu (II) concentrations ranging from 3.81 to 18.14 $\mu\text{g L}^{-1}$,
126 Fe (III) ranging from 0.12 to 8.42 $\mu\text{g L}^{-1}$ and Al (III) ranging from 0.09 to 11.13 $\mu\text{g L}^{-1}$. These
127 findings underscore the environmental significance of these metallic ions in these aquatic
128 environments (Constantino et al., 2019).

129 For this study, we evaluated the characterization and binding ability of AHS with metal ions
130 from two sites: the Negro River, located in Manaus (capital of Amazonas state, Brazil), near an
131 urbanized area, and the Carú River, in the city of Itacoatiara (Amazonas, Brazil), the second most
132 populous city in the state, located approximately 270 km from the state of the capital (BRASIL,
133 2023). The assessment of the interaction between Aquatic Humic Substances (AHS) and metallic
134 ions can provide insights into the availability and transport dynamics in the main rivers of the
135 Amazonian region. Understanding this interaction is important for predicting the vulnerability of
136 aquatic life and comprehending the complex environmental processes occurring in these
137 ecosystems.

138 In addition to the concentration-dependent relationship of organic matter in decreasing the
139 availability of certain metal ion species, factors such as heterogeneity and structural aspects have

140 influence and must be evaluated for a better understanding of the organic matter-metal interaction.
141 (Al-Reasi et al., 2011). Thus, the determination of complexation capacity (CC) of the aquatic bodies
142 help to predict how much of either expect and unexpected entry of metals can be complexed or free
143 to the aquatic environment. Considering the influence of AHS chemical composition on metal ions
144 in the aquatic environment, and the scarcity of study in the region of Itacoatiara city, this study
145 aimed to assess (i) the molecular features of AHS from blackwater Amazonian rivers of Negro and
146 Carú rivers (seasonal sampled) and (ii) to combine the use CP-PARAFAC and 2D-COS FTIR to
147 evaluate their interactions with Fe (III), Al (III) and Cu (II).

148

149 **Material and Methods**

150 AHS isolation

151

152 Three AHS samples used in the study were extracted from two blackwater rivers located in
153 the Central Amazon basin (Amazonas, Brazil): Carú river (03°02'21.7''S 058°37'27.9''W) sampled
154 in dry season (RC-I - November) and rainy season (RC-II - July), located at Itacoatiara city, and the
155 Negro river (03°02'22''S 060°08'21''W) (RN – dry season), the main blackwater river in this
156 watershed, located near Manaus (Sampling authorization: SISBIO n° 50042-2).

157 The surface water was initially filtered utilizing a qualitative filter to remove leaves and
158 branches and then acidified to pH 2.0 with HCl 6.0 mol L⁻¹, as previously described by Constantino
159 et al. (2021). HS were isolated using Superlite DAX-8 resin (Sigma-Aldrich) and eluted with a 0.1
160 mol L⁻¹ NaOH solution, as recommended by International Humic Substances Society (IHSS) and
161 purified using a cation exchange resin (Dowex 50WX8, hydrogen form, 200-400 mesh, Sigma-
162 Aldrich) (Maurice et al., 2002; Thurman & Malcolm, 1981).

163

164 AHS characterization

165

13

14

166 AHS were characterized using ^{13}C Solid State Nuclear Magnetic Resonance Spectroscopy
167 (^{13}C -CPMAS-NMR) and Thermally methylation assisted hydrolysis reactions coupled to gas
168 chromatography and mass spectrometry (TMAH-Thermochemolysis GC-MS).

169
170 Solid State Nuclear Magnetic Resonance Spectroscopy (^{13}C -CPMAS-NMR)

171
172 ^{13}C -CPMAS-NMR were acquired employing a Bruker AV-300 MHz (Bruker, Billerica,
173 MA, USA), equipped with a Magic Angle Spin (MAS) probe with widebore of 4.0 mm. The carbon
174 spectra were obtained from a rotation frequency in the rotor of 10 KHz, 1 s of recycle time, 1
175 millisecond of contact time, 20 milliseconds of acquisition time and 4000 scans. Zircon cylindrical
176 rotors, 4.0 mm diameter, were packed with about 80 mg of the sample and sealed with a Kel-F®
177 cap. The ^{13}C -CPMAS-NMR spectra was divided into the following main regions: alkyl-C (0–45
178 ppm); methoxyl-C and N-alkyl-C (45–60 ppm); O-alkyl-C (60–110 ppm); unsubstituted and alkyl-
179 substituted aromatic-C (110–145 ppm); O-substituted aromatic-C (145-160 ppm); carboxyl-C (160–
180 190 ppm). Each region describe above was divided by the sum of all spectral zones, to obtain a
181 relative amount in relation to the total spectra (MestreNova 6.2.0 software, Mestre-lab Research,
182 2010).

183
184 Thermochemolysis GC-MS

185
186 TMAH-Thermochemolysis GC-MS was performed in the AHS, with 80 mg of each sample.
187 The samples were placed in a quartz tube and were added 300 μL of tetramethylammonium (25% in
188 methanol). After the mixture dried, the sample were introduced into a Pyrex tubular reactor under a
189 Tube Furnace model F21100 and heated at 400 $^{\circ}\text{C}$ under a helium flow. The products released from
190 Thermochemolysis were continuously transferred into two successive chloroform traps, which they
191 were combined and concentrated by rotoevaporation. The products, released and concentrated, was

192 recovered and adjusted to a final volume of 500 μL with chloroform in a vial which followed to
193 GC-MS analysis (PerkinElmer, Auto System XL) using a RTX-5MS WCOT capillary column,
194 (Restek, 30 m \times 0.25 mm; film thickness, 0.25 μm) that was coupled to a PE Turbomass-Gold
195 quadrupole mass spectrometer, as previously described by (Bento et al., 2020, 2021). The
196 chromatograms were submitted to interpretation according NIST database.

197

198 Interaction studies with metallic ions utilizing Parallel Factor Analysis (PARAFAC) and Ryan
199 Weber model

200

201 For the interaction assays, solutions with AHS of 10.0 mg L^{-1} of dissolved organic carbon
202 (DOC) were prepared adjusted by a Total Organic Carbon analyzer (Shimadzu, TOC-VCSN,
203 Japan). The pH was adjusted to 6.0 using 0.1 mol L^{-1} NaOH or 0.1 mol L^{-1} HCl solutions for all sets
204 of samples (Huang et al., 2018) . Titrations of the metals ions Cu (II), Al (III) and Fe (III) were
205 performed by the addition of stock solutions (5.0, 25.0 and 1000.0 mg L^{-1}), resulting in final
206 concentrations ranging from 5.0—5000.0 $\mu\text{g L}^{-1}$ for each cation in a final volume of 25.0 mL. The
207 solutions were kept under stirring (200 rpm) on a shake table, for 24 hours to ensure the
208 coordination equilibrium (Huang et al., 2018; Soares da Silva et al., 2020)

209 After this preparation, fluorescence quenching combined with Parallel Factor Analysis
210 (PARAFAC) was made performed following the literature procedure, as a multi-response method to
211 evaluate the complexation of the AHS. For this, Emission Excitation Matrix (EEM) fluorescence
212 spectra of AHS solutions were acquired with the different metal ion concentrations, using a
213 Spectrofluorimeter Lumina (ThermoScientific) (Tadini et al., 2020). The samples of AHS from the
214 Carú and Negro rivers had their absorbance adjusted to 0.2 at 254 nm to avoid the inner filter effect
215 (Carstea et al., 2020; Luciani et al., 2009). The excitation and emission slits were fixed at 5 nm.
216 Excitation ranged from 220 to 520 nm and emission wavelengths ranged from 250 to 600 nm, with
217 a scan speed of 2400 nm min^{-1} and detector voltage of 600 V. Additionally, the diffusion signals

17

18

218 from the EEM spectrum were removed using Rayleigh scattering by cutting the diffusion band at 15
 219 nm and applying the Zepp method to remove first- and second-order Raman scattering (Mounier et
 220 al., 2011; Zepp et al., 2004) using the PROGMEEF software (Redon & Mounier, 2018) in Matlab
 221 language. The number of components evaluated ranged from 2 to 5 within the spectral range of 220
 222 to 520 nm for excitation and 250 to 600 nm for emission. The best components recognized for core
 223 consistency diagnostics (CORCONDIA) were above 60% (Mounier et al., 2011). This approach
 224 provides detailed information about each fluorescent component present in the sample and their
 225 interaction with the metal ions through fluorescence suppression.

226 The concentration of binding sites (L_T) and the conditional constant stability (K_{ML}) of the
 227 complex (AHS-M) of each fluorophore were determined using a nonlinear fitting model proposed
 228 by Ryan and Weber (1982). The assumes a 1:1 interaction, considering one ligand site with one
 229 metal ion. The suppression of fluorescence intensity (I) caused by the concentration of the added
 230 metal (C_M in mol L⁻¹) is related with the total ligand concentration (L_T in $\mu\text{mol-M L}^{-1}$). The
 231 fluorescence intensity of the unbound ligand allows the determination of the conditional constant
 232 stability of the complex (K_{ML}) and the total ligand site concentration (L_T in $\mu\text{mol-M L}^{-1}$) as
 233 described by Equation 1. I_{ML} is the limit value below which the fluorescence intensity does not
 234 change due to the addition of metal.

$$235 \quad I = \left(\frac{I_{ML} - 100}{2 K_{ML} L_T} \right) \left[\left(K_{ML} L_T + K C_M + 1 \right) - \sqrt{\left(K_{ML} L_T + K_{ML} C_M + 1 \right)^2 - 4 K^2 L_T C_M} \right] + 100 \quad (1)$$

236
 237 Briefly, Equation 2 illustrates the interaction of free metal (M) with a free complexing site
 238 (L), forming a complex (ML). The mass balance of the chemical reactions and the equilibrium
 239 constant stability (K_{ML}) are represented by the Equations 3—5.



$$241 \quad L_T = [ML] + [L] \quad (3)$$

$$242 \quad C_M = [ML] + [M] \quad (4)$$

243
$$K_{ML} = \frac{[ML]}{[M][L]} \quad (5)$$

244 The complexation capacity, referred to here as CC (in $\mu\text{mol-M mg}^{-1}$ DOC), was defined as
245 the quotient of binding sites concentration (L_T) by the DOC of each sample, as described by
246 Equation 6 (Soares da Silva et al., 2020; Tadini et al., 2020).

247
$$CC = \frac{L_T}{[DOC]} \quad (6)$$

248

249 Two-dimensional correlation spectroscopy

250

251 To acquire information about the possible structural changes resulting from the interaction
252 of metal ions and AHS, the two-dimensional correlation spectroscopy (2D-COS) was applied using
253 Fourier Transformed Infrared (FTIR) measurements (Huang et al., 2018; Santos et al., 2021; Soares
254 da Silva et al., 2020). After the interaction studies, the samples were freeze-dried and were
255 dissolved in H₂O:Methanol (40:60 μL), then carefully dropped into ATR crystal and evaporated to
256 dryness under N₂ flow (Santos et al., 2021; Soares da Silva et al., 2020). Thus, the FTIR spectra
257 were acquired in ATR mode with a 400 to 4000 cm^{-1} scan and a resolution of 4 cm^{-1} (Spectrum
258 Two UATR, Perkin Elmer, USA). The analysis of set of FTIR data was analyzed in synchronous
259 and asynchronous modes to evaluate the spectral variation induced by increasing metallic additions
260 (external perturbation) into AHS solutions. Synchronous and asynchronous spectra were generated
261 using OriginPro 2024 with the 2D Correlation Spectroscopy Analysis toolbox.

262

263 **Results and Discussion**

264 Aquatic humic substances characterization

265

266 RC and RN AHS were previously characterized and reported by Constantino et al (2021).
267 Briefly, elemental analysis (CHNS) indicated that RC-I and RC-II had higher %N, 1.6 and 1.1,
268 respectively. The lower C/N ratio was associated with the less humified material, with results of
269 74.52, 25.75 and 46.79, for RN, RC-I and RC-II, respectively. These results suggested that the
270 material from RN was more humified, and a seasonal effect between RC samples. RC-I was
271 extracted during a flooded period of the region's sampling, suggesting a higher incorporation of the
272 humified soil material leached into this river. FTIR analysis highlighted the presence of C=O bands
273 (1700 cm^{-1}) for RC samples. More details of the characterization of these AHS can be found in the
274 cited reference.

275 ^{13}C -CPMAS-NMR

276

277 The ^{13}C -CPMAS-NMR spectra acquired for AHS from RC-I, RC-II and RN are shown in
278 Figure 1S. The spectra showed a complex mixture in the samples, featuring aromatic and aliphatic
279 moieties, with the most prominent presence of aliphatic moieties in the aquatic samples (Kögel-
280 Knabner, 1997; Tadini et al., 2015). The resonant carbon nucleus in the region of 0-45 ppm is
281 correlated to the carbon of alkyl chains ($-\text{CH}_3$ and $-\text{CH}_2$). The peak at 30 ppm can be correlated to
282 long C-alkyl chains of lipids, such as plant waxes and polyesters (Bento et al., 2020; Soares da Silva
283 et al., 2020; Verrillo et al., 2021).

284 The resonant region of 45-60 ppm is correlated to O- CH_3 and C-N moieties. The peaks at 53
285 and 54 ppm are assignments of methoxy, derivate from lignin units (guaiacyl and syringyl);
286 Furthermore, the presence of these peaks in this region can be ascribed to polysaccharides
287 (hemicelluloses) and some contribution of C-N binding of peptides and amino acids (Spaccini et al.,
288 2019; Verrillo et al., 2021).

289 The region from 60-90 ppm is mostly attributed to O-Alkyl of polysaccharides. In the region
290 of 110-160 ppm, the peaks can be attributed to the presence of aromatic carbon, such as compounds

291 derived from the degradation of lignin; The range from 145-160 ppm represents the resonance of O-
292 Aryl moieties, such as in the phenolic or methoxyl moieties from lignin (ether bond). The peak at
293 172 ppm in the range of 160-190 ppm is from the resonance of carboxylic acids, showing a greater
294 area correlated to this chemical function (Dignac et al., 2003).

295 The integration of the relative areas from each region in the spectra allowed differentiation
296 of the character of the molecular structure based on the distribution of the carbon resonance.
297 Additionally, indexes such as Aromaticity ratio (AR), Lignin ratio (LR) and Hydrophobicity index
298 (HI) (Table 1) were used to predict the aromaticity, presence of lignin and aliphatic content,
299 respectively.

300 RC-I showed the highest aromaticity (23.6). The higher area in the resonant carbon region
301 of 45-60 ppm (relative to C-methoxy/amino acids) compared to 145-160 ppm (O-Aryl) resulted in a
302 higher LR index, suggesting that the origin of aromatic units is not from lignin and may be derived
303 from microbial activity or other autochthonous sources. However, the aromatics moieties that
304 comprised the AHS arrangement of RC-II are mainly derived from lignin (lower LR index)
305 indicating the allochthonous influence.

306 The hydrophobicity index is used to assess the biochemical stability of organic matter
307 (Bento et al., 2021). Although the values are not so different (Table 1), the contribution between the
308 aromatic and aliphatic carbon resonances changed during the seasons. In RC-I, the major
309 contribution was from the resonance of aromatic carbon (140-110 ppm), while for RC-II, it was
310 aliphatic carbons.

311 The structural indexes and the integrative area analysis highlighted the differences between
312 AHS from RC-I and RC-II. In the dry season, AHS from RC-I appeared more aromatic, resulting
313 from the preservation of aromatic moieties and products derived from aquatic organisms
314 (autochthonous). On the other hand, in the rainy season, the main contribution to the AHS
315 composition came from the new input of fresh organic matter carried from the soil by the rain, such
316 as lignin and polysaccharide structures (allochthonous).

317 The study by Oliveira et al (2007), evaluating AHS sampled in the rainy season from the
 318 Negro River, found a major contribution in the resonance of carbon related to alkyl, methoxy, and
 319 N-alkyl moieties of 47.9 (0-65 ppm) and an aromatic contribution of 9.2 (110-165 ppm), while in
 320 the dry season, the respective contributions were 36.6 and 18.5. Thus, the study corroborates with
 321 the results reported here, indicating a greater input of alkyl moieties in the rainy season and the
 322 prevalence of aromatic character during the dry season.

323

324 **Table 1** Integrated relative areas (%) along the chemical shift of the main peaks (ppm) of ¹³C-
 325 CPMAS-NMR spectra of AHS isolated from Amazonian blackwaters.

	Spectrum allocation (ppm)						Indexes		
	190-160	160-140	140-110	110-60	60-45	45-0	AR ^a	LR ^b	HI ^c
	C=O	O-Aryl	Aryl	O-Alkyl	O-C/ C-N	Alkyl			
RC- I	6.2	3.6	17.4	22.4	14.6	35.6 7	23. 6	4.0	1.3
RC- II	15.5	9.3	13.8	17.4	6.7	37.2 6	19. 1	0.7	1.4
RN	5.7	4.8	16.8	32.5	12.9	27.2 2	22. 7	2.7	0.9

326 ^aAR: Aromaticity ratio: [(110—160 ppm)/(0—190 ppm)] x100

327 ^bLR: Lignin ratio: (45—60)/(145—160)

328 ^cHI: Hydrophobicity index: [Σ(0-45 ppm)+(110-160 ppm)]/Σ[(45-60 ppm)+(60-110 ppm)+(160-190 ppm)].

329

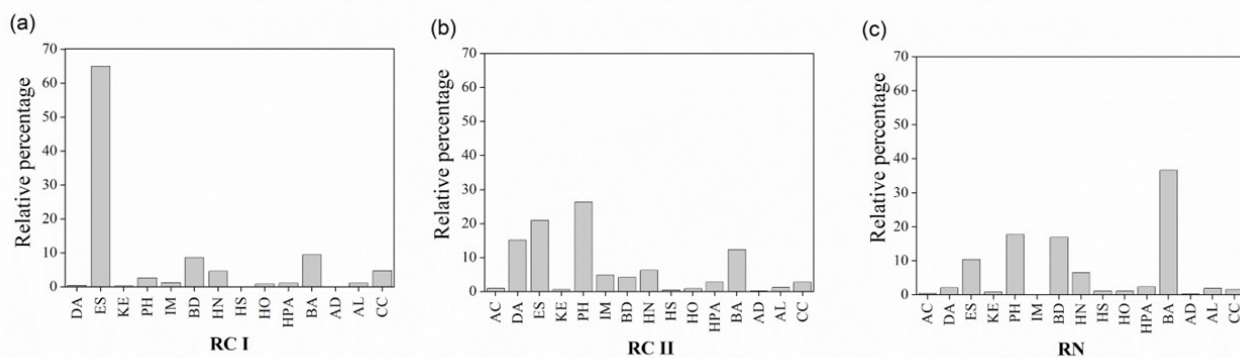
330 Thermochemolysis GC-MS

331 Figure 1 displays the relative intensity of the products released from Thermochemolysis GC-
 332 MS for all AHS samples. The chromatograms and the identified compounds are summarized in
 333 Figure 2S and Table 1S of Supplementary Material, respectively.

334 The main classes identified for RC-I were aliphatic ester (ES), benzene derivatives (BD) and
 335 benzoic acids (BA), while for RC-II and RN the identified classes included dicarboxylic acid (DB),
 336 aliphatic ester (ES), phenolic compounds (PH), benzene derivatives (BD) and benzoic acids (BA)
 337 (Fig. 1).

27

28



338

339 **Fig. 1** Relative percentage (%) of classes of compounds identified by Thermochemolysis GC-MS of
 340 AHS in (a) RC-I, (b) RC-II and (c) RN. DA= Dicarboxylic acids; ES= aliphatic ester; KE=
 341 ketones; PH=phenol; IM=imines; BD= benzene derivatives; HN= Heterocyclic nitrogen; HS=
 342 Heterocyclic sulfur; HO=heterocyclic oxygen; BA= benzoic acids; AD=Amides;
 343 AL=Alkanes/alkenes/alkynes; CC=cyclic compounds.

344 Representative of the dry season, RC-I presented a molecular structure composed mainly by
 345 ES, from the fatty acids, as well as the accumulation of hydrocarbons (alkanes and alkynes) from
 346 plant tissues (i.e. cutin and suberin). Additionally, some hydrocarbons C₂₁, C₃₃, C₁₄-C₁₉ are derived
 347 from microbial activity, while C₂₀-C₃₂ originated from plant tissues (Tadini et al., 2015).

348 Benzene derivatives and phenolic compounds detected in RC-II and RN are mainly derived
 349 from the lignin monomers (hydroxyphenyl, guaiacyl and syringyl) (Bento et al., 2020; Nebbioso &
 350 Piccolo, 2012; Tadini et al., 2015), typical of allochthonous organic matter. Furthermore, in the RC-
 351 II and RN (rainy season) the compounds seem more diluted, because chromatograms (Figure 2S,
 352 Supplementary Material) reveal lower intensities and the same AHS weight was employed for
 353 Thermochemolysis analysis. In contrast, RC-I showed fewer compounds but larger intensities.

354 As pointed out by ¹³C NMR, RC-I was mostly influenced by autochthonous organic matter
 355 (aromatic not derivate from lignin), while the RC-II and RN showed more influence of
 356 allochthonous organic matter (aromatics from lignin). However, Thermochemolysis showed mainly
 357 aliphatics moieties in the dry season (RC-I) from plant tissues and microbial activity, while in the
 358 rainy season (RC-II), there was a contribution of phenols and benzenes derivatives.

29

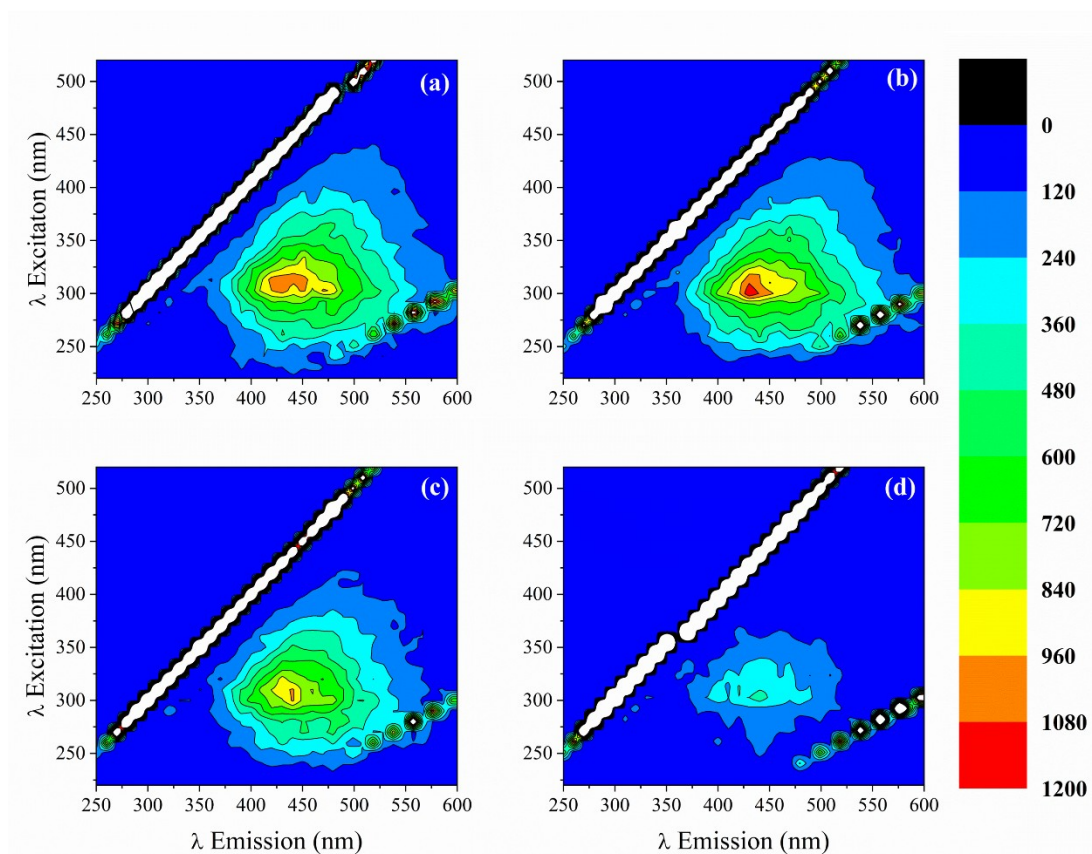
30

359 The different responses can be related to the structural variations of AHS caused by
360 seasonality, and the responses from these two different analytical techniques. The higher
361 aromaticity of RC-I as pointed by aromaticity index (Table 1) in relation to RC-II and RN, did not
362 release aromatic products during the Thermochemolysis process. This is because aromatic moieties
363 have greater thermal stability (Rosa et al., 2012).

364 Furthermore, the ^{13}C NMR spectra of RC-I showed a thinner peak at 130 ppm compared to
365 the other AHS; this peak can suggest the uniformity/presence of the same compounds by
366 intensifying the peak and decreasing its width, while the larger ones can suggest a more
367 heterogeneous molecular structure, i.e. in RC-I the aromatic units may be more linear
368 polycondensated (higher thermostability). Furthermore, the polyhydroxy compounds can undergo
369 pyrolytic rearrangement during the Thermochemolysis GC-MS and are detectable as aromatic
370 moieties. For instance, the polysaccharides (O-Alkyl) pointed out by ^{13}C NMR in RC-II and RN can
371 undergo pyrolytic rearrangement and aromatization, being detectable as benzene derivatives and
372 phenols. This confirms the fact that the AHS from the rainy season comprised a molecular structure
373 with a higher contribution of terrestrial input.

374
375 Behavior of AHS fluorophores with Cu(II), Al(III) and Fe(III) and binding parameters

376
377 The interaction of AHS extracted from Amazonian rivers with the metal ions was evaluated
378 through fluorescence suppression. Figure 2 illustrates the changes in the EEMs fluorescence spectra
379 for the AHS RN in the presence of different Cu (II) concentrations, compared to the control (AHS
380 RN in the absence of Cu (II)). It is possible to observe that with an increase in Cu (II)
381 concentrations there is a suppression of maximum fluorescence intensity (F_{max}). The addition of 5.0
382 mg L^{-1} Cu (II) caused the suppression of approximately 55% of the F_{max} , along with a slight shifting
383 of the main peak (F_{max}) ($\lambda_{\text{ex}}/\lambda_{\text{em}} = 313/430 \text{ nm}$).



384

385 **Fig. 2** Contour EEMs maps of the AHS RN with Cu (II) additions at pH 6.0: (a) control; (b)
 386 addition of 50 $\mu\text{g L}^{-1}$ Cu (II) (c) addition of 500 $\mu\text{g L}^{-1}$ Cu (II) and (d) addition of 5000 $\mu\text{g L}^{-1}$ Cu
 387 (II).

388

389 Aiming to understand the interactions of AHS and metal ions, the EEM spectra were
 390 statistically analyzed with CP-PARAFAC, which was able to provide information about the single
 391 components contributing to the fluorescence signals in AHS. The assessment of the best number of
 392 fluorescent components obtained by CP-PARAFAC was done through the analysis of the core
 393 consistency diagnostic values (CORCONDIA). In general, for all AHS samples, optimum
 394 CORCONDIA values ($> 60\%$) were obtained for two components, for which the values were
 395 96.3%, 87.2% and 88.7%, for RC-I (n=14), RC-II (n=14) and RN (n=14), respectively.

396 In this study, the components were named as C1, for component 1 and C2, for component 2;
 397 and they showed a very resemble fluorescence profile (Figure 3S), which was classified as typical
 398 humic peaks (Coble et al., 2014). For all quenching experiments, C1 showed higher fluorescence

33

34

399 intensities in the blue region of the emission wavelength ($\lambda_{\text{ex}}/\lambda_{\text{em}} \sim 310/420$ nm), suggesting the
400 presence of a fluorophore comprising more aliphatic character (Bento et al., 2020; de Morais et al.,
401 2021; Funkey et al., 2019; Soares da Silva et al., 2020). On the other hand, C2 presented a longer
402 shift in relation to C1, with maximum fluorescence intensity at longer wavelengths ($\lambda_{\text{ex}}/\lambda_{\text{em}} \sim$
403 $310/470$ nm) for all samples, slightly red-shifted for RN ($\lambda_{\text{ex}}/\lambda_{\text{em}} = 300/490$ nm).

404 The red shifting effects in fluorescence can result from the presence of highly conjugated
405 systems; in addition, the lower fluorescence intensities observed for C2 can be assigned to the
406 presence of electron-donating substituents as well (Coble et al., 2014; De Mastro et al., 2019;
407 Senesi et al., 1991; Traversa et al., 2014). The maximum fluorescence intensities of the components
408 are shown in Table 2. In general, the F_{max} obtained for C1 and C2 followed this AHS order: RC-I >
409 RC-II > RN.

410

411

412

413

414

415

416

417

418

419

420

421

422

423

424

35

36

425 **Table 2** Maximum Fluorescence intensities (F_{max}) and binding parameters of interactions of AHS
 426 components (C1 and C2) with Cu (II), Al (III) and Fe (III): BIAS, binding site concentration (L_T),
 427 conformational stability constant (K_{ML}) and complexation capacity (CC).

		C1						C2						CC _{Total} *
		F_{max}	BIAS	L_T ($\mu\text{mol L}^{-1}$)	K_{ML} ($\times 10^5$)	$\log K_{ML}$	CC (mmol g^{-1} DOC)	F_{max}	BIAS	L_T ($\mu\text{mol L}^{-1}$)	K_{ML} ($\times 10^5$)	$\log K_{ML}$	CC (mmol g^{-1} DOC)	
Cu (II)	RC-I	141 7	1.94	20	3.2	5.5	2.0	645	2.15	4	5.0	5.7	0.4	2.4
	RC-II	114 4	1.06	5	4.0	5.6	0.5	776	1.43	4	5.0	5.7	0.4	0.9
	RN	805	0.78	15	6.3	5.8	1.5	456	3.47	7	10.0	6.0	0.7	2.2
Al (III)	RC-I	147 4	1.07	25	7.9	5.9	2.5	821	0.91	15	1.5	6.2	1.5	4.0
	RC-II	120 0	0.59	20	5.0	5.7	2.0	778	0.91	15	7.9	5.9	1.5	3.5
	RN	815	nd	nd	nd	nd	Nd	416	nd	nd	nd	nd	nd	nd
Fe (III)	RC-I	140 3	0.70	30	0.3	4.5	3.0	688	0.48	13	3.1	5.5	1.3	4.3
	RC-II	127 5	0.94	20	0.8	4.9	2.0	677	2.80	26	3.1	5.5	2.6	4.6
	RN	865	2.42	70	0.8	5.9	7.0	472	11.5	50	5.0	5.7	5.0	12.0

428 (nd) not determined

429 (*) Total complexation capacity: Sum of CC of each component in mmol g^{-1} DOC

430

431 The binding parameters of the interactions AHS-M obtained in the quenching experiments,
 432 for each component were quantitatively described by the complexation model proposed by Ryan
 433 and Weber (1:1/ligand:metal)(Ryan & Weber, 1982).

434 Figure 3 shows the titration curves of the quenching experiments of RC-I, RC-II and RN
 435 with Cu (II), for each fluorescent component. The titration curves for Al (III) and Fe (III) assays are

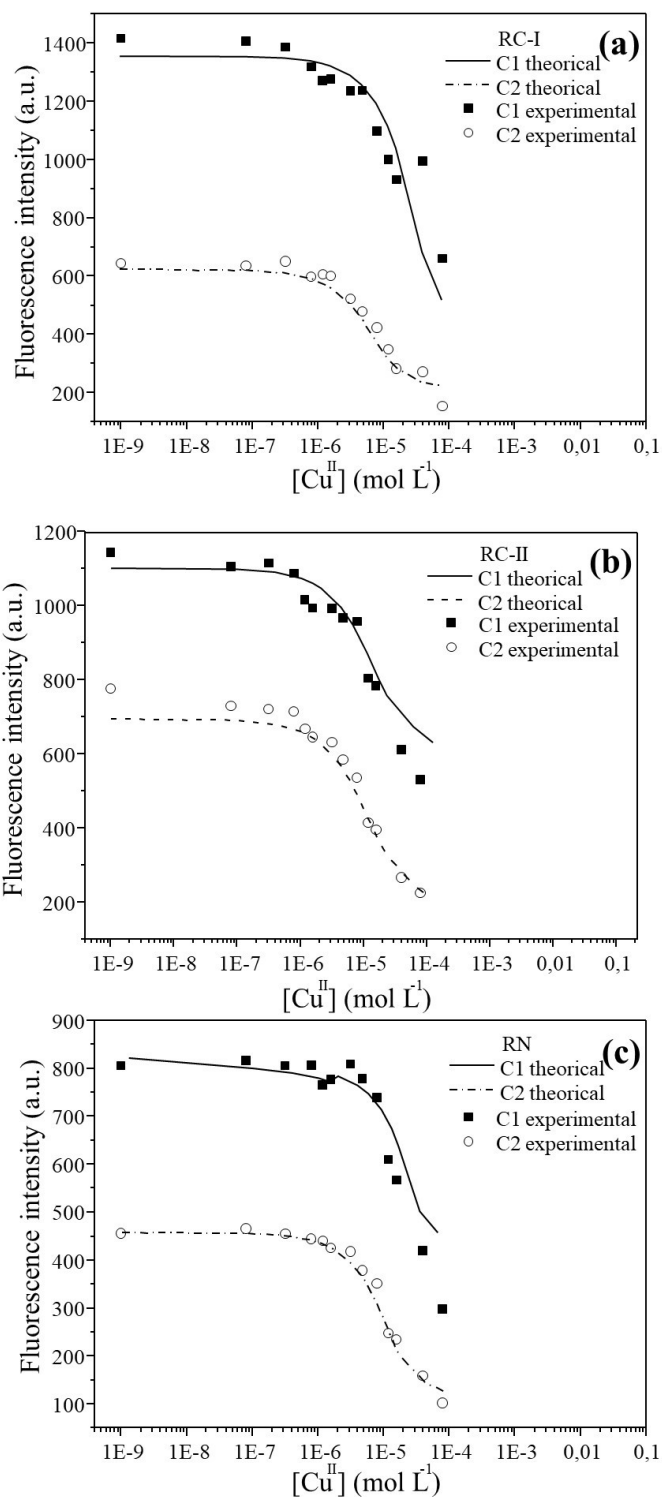
37

19

38

436 illustrated in Figure 4S and 5S (see Supplementary Material). Fluorescence suppression appears to
437 be more intense in the first Cu (II) additions, which can be related to the presence of free or
438 unsaturated binding sites. The quenching becomes weaker as Cu (II) increments are made,
439 indicating a decrease in the concentration of reactive sites caused by the steric effects of the
440 complexed sites.

441



442

443 **Fig. 3** Fluorescence quenching of components 1 and 2 of AHS from RC-I (a), RC-II (b) and, RN (c)

444 with Cu (II) titration at pH 6.0. The symbols represent the data obtained experimentally for C1 (■)

445 and C2 (○) and the lines for C1 (—) and C2 (---) represent the theoretical values, with the

446 concentration axis plotted in a logarithmic scale (\log_{10}).

41

42

447
448 For the assessment of the data fitting to the model used for complexation, the BIAS, which
449 represents the error between the model and experimental values, was used. It is the absolute sum of
450 the difference between the values of the experimental fluorescence intensity logarithms and the
451 theoretical values (Mounier et al., 2011) .

452 Good adjustments were obtained between the experimental data and the values calculated
453 by the 1:1 model (Table 2). In the complexation assays, the BIAS values ranged from 0.48 to 3.47,
454 indicating that the experimental data fitted well with the theoretical model, except for the test
455 performed with Fe (III) and AHS RN (only for C2), in which the BIAS was 11.5 (Figure 4S). In the
456 Al (III) and AHS RN assay for both components, the data did not fit the one ligand model (Figure
457 5S), indicating that more than one ligand site may be acting simultaneously with the Al (III)
458 complexation and should be further investigated.

459 The binding parameters determined were the conformational stability constant (K_{ML}), the
460 binding sites concentration (L_T) and the complexation capacity (CC) (Table 2). The complexation
461 results obtained for the AHS in this study agree with the literature data (Antunes et al., 2007;
462 Nebbioso & Piccolo, 2009). The stronger ligands are those with binding site concentrations (L_T)
463 around 10^{-6} mol L⁻¹ and conformational stability constant (K_{ML}) around 10^5 (Antunes et al., 2007;
464 Mounier et al., 2011). The K_{ML} obtained in this study ranged from 3.0×10^4 to 1.0×10^6 , and the L_T
465 concentrations ranged from 4.0×10^{-6} to 7.0×10^{-5} mol L⁻¹ (Table 2).

466 In comparison to the individual results of each component, in all complexation assays, C2
467 showed higher stabilities (K_{ML}) than C1 for the complexes formed, except for RC-I in the Al (III)
468 assay. This can be explained by characteristics such as aromaticity since the C2 had the lower
469 energy emission peak (longer wavelengths) among the AHS samples studied here. However, C1
470 showed the highest CC than C2, which C1 comprises a more aliphatic character. The results suggest
471 that aliphatic structures play an important role in metal interactions than aromatics, but the
472 aromatics form a more stable complex than aliphatic.

473 Previous studies have already indicated that saturated and unsaturated long-chain alkanolic
474 acids interact with metals more easily due to their molecular flexibility than a supramolecular
475 structure comprising aromatic moieties. However, as observed in these studies, the complex formed
476 by aliphatic moieties did not show higher stability (K_{ML}) than the aromatic one (Table 2), suggesting
477 that this kind of complex can be easily disrupted (Nebbioso & Piccolo, 2009).

478 The variability of CC does not depend solely on the molecular composition but also on the
479 supramolecular architecture that AHS presents, which was evaluated by the available binding sites
480 (L_T). The complexation capacity (CC) here was calculated as the concentration of binding sites per
481 gram DOC (Tadini et al., 2020). In an environmental context, the CC of AHS can indicate the
482 availability and toxicity of metallic ions in the environment. Thus, a high CC may suggest reduced
483 availability of these ions and, consequently, lower toxicity, particularly for aquatic organisms
484 inhabiting these environments (Kungolos et al., 2006; Yang et al., 2021). The total CC showed that
485 the AHS interacted more with Fe (III) > Al (III) > Cu (II), suggesting that AHS can interact with Fe
486 (III) and Al (III) when their input is larger (rainy season). Conversely, it indicates that AHS may not
487 interact equally with Cu (II) when there is a large input, e.g. due to anthropogenic actions, leaving
488 this metal more available for aquatic organisms.

489 In a study of AHS sampled from the Turvo-Grande basin (São Paulo state-Brazil), the
490 complexation capacities of AHS from agricultural and urban areas with Cu (II) and Ni (II) were
491 evaluated. For Cu (II), the stability of the complexes formed ($\log K_c$) was lower than in the present
492 study and varied from 0.04 to 1.35. The CC ranged from 0.07 mmol g⁻¹ DOC (agricultural area) to
493 29.5 mmol g⁻¹ DOC (urban area). This study also showed that AHS from urban areas had a more
494 functional complexity and was related to complexation capacity (Tadini et al., 2013).

495 Studies comparing two methods in the evaluation of the complexation capacity of aquatic
496 and terrestrial organic matter with Cu (II), including a sample extracted from the Negro River,
497 showed similar results for $\log K_c$ (4.22) and CC of 1.44 mmol g⁻¹ DOC (Romão et al., 2003).

498
45
46

499 Two-dimensional Correlation Spectroscopy

500

501 The FTIR spectra after the quenching assays were analyzed with 2D-COS for the assessment
502 of the perturbation of the metals caused in the functional groups involved in the complex formation
503 (AHS-M), covering all chemical functionalities present in the samples, whether fluorescent or not
504 (Huang et al., 2018; Soares da Silva et al., 2020). Figure 6S shows the changes in the FTIR spectra
505 for the AHS in the presence of different metal ion concentrations. For the interpretation the region
506 of 1800 to 900 cm^{-1} of maps was used to assign the functional groups that interact with the metal
507 ions tested, and Figures 7S, 8S and 9S show the 2D-COS contour maps, synchronous and
508 asynchronous, and provide information about the order of events that occurred in the AHS with the
509 Cu (II), Al (III) and Fe (III) addition. Table 3 summarizes the autopeaks of synchronous and cross
510 peaks of asynchronous maps for RC-I, RC-II and RN.

511

512

513

514

515

516

517

518

519

520

521

522

523

524

47

48

525 **Table 3** Autopeaks of synchronous and cross peaks of asynchronous mode and changes in the
 526 chemical groups found for RC-I, RC-II and RN with Fe (III), Al (III) and Cu (II) addition.

Metallic ion	Sample s	Synchronous (cm⁻¹)	Asynchronous (v₁, v₂) (cm⁻¹)	The sequence of changes in the chemical groups by the metal addition
Cu (II)	RC-I	1275	(1260,1330) - (1260,1600) +	C-O _{phenolics} > O-H _{phenolics} > N-H _{amines, amides}
	RC-II	1317	(1330, 1400) + (1330, 1600) +	C-O _{phenolics} > N-H _{amines, amides} ≈ COO ⁻
	RN	1350 1580	(1600,1370) - (1600,1260) +	COO ⁻ > N-H _{amines, amides} > O-H _{phenolics}
Al (III)	RC-I	1330	(1330, 1400) + (1330, 1600) +	C-O _{phenolics} > COO ⁻ > N-H _{amines, amides}
	RC-II	1252 1600	(1280,1600) +	O-H _{phenolics} > N-H _{amines, amides}
	RN	1296 1600	(1300,1370) -	COO ⁻ > C-O _{phenolics}
Fe (III)	RC-I	1350	(1370,1600) +	COO ⁻ > N-H _{amines, amides}
	RC-II	1336	(1330, 1400) - (1330, 1600) +	COO ⁻ > C-O _{phenolics} > N-H _{amines, amides}
	RN	1319	(1330, 1370) -	COO ⁻ > C-O _{phenolics}

527 (+) refers to autopeak positive above the principal diagonal.

528 (-) refers to autopeak negative above the principal diagonal.

529

530 In all samples, in the synchronous map of interaction with Cu (II), Fe (III) and (Al (III), the
 531 wavenumbers between 1275 and 1350 cm⁻¹ are evident. In studies of humic substances, this region
 532 is usually associated with C-O stretching and O-H bending deformation of phenolic groups (Chen et
 533 al., 2014; Yuan et al., 2018). For the sample RN in the interaction with Al (III) and Cu (II), the
 534 region near 1600 cm⁻¹ is commonly associated with the N-H bend of primary and secondary amines
 535 and amides (Chen et al., 2015; Luo et al., 2022; Pavia et al., 2008).

536 On the asynchronous map, it is possible to identify the sequence of events that occurred
537 during system disturbance, i.e., the sequence of functional groups where Cu (II) interacted
538 preferentially, following Noda's Rule (Noda & Ozaki, 2004).

539 For the asynchronous map, the bands located between 1260-1280 cm^{-1} are attributed to O-H
540 stretching in phenolics, 1300-1330 cm^{-1} to C-O stretching in phenolics, 1370-1400 cm^{-1} to COO^-
541 asymmetrical stretching, and 1600 cm^{-1} of N-H bends of amines and amides (Chen et al., 2015; Li et
542 al., 2017). The sequence of changes in the chemical groups due to the metallic ion addition is shown
543 in Table 3.

544 These results suggest that phenolics groups (C-O and O-H) initially undergo metal binding
545 and rearrangements for RC-I and RC- II with Cu (II) and Al (III), exposing other functional groups
546 such as carboxylate to metal complexation via intermolecular reactions, generating
547 thermodynamically more stable structures, since the complexation occurs in a way to form complex
548 thermodynamically more favorable. However, in all samples, these groups participate in the
549 interaction, which is consistent with the findings from Thermochemolysis GC-MS analysis,
550 indicating that all AHS contain phenolic moieties in composition (Nebbioso & Piccolo, 2009).
551 These findings also corroborate with the behavior identified by the PARAFAC analysis in the
552 complexation assays, where aliphatic domains presented in the C1 component were attributed to
553 higher complexation capacities, while phenolic domains were assigned to form more stable
554 complexes.

555 Additionally, in these samples, it is possible to observe the interaction of N-H groups of
556 amines and amides with the same metallic ions. This is consistent with the elemental analysis of
557 these materials previously published, which indicated that RC-I (C/N=25.75) and RC-II
558 (C/N=46.79) had higher nitrogen content than RN (C/N = 74.52) (Constantino et al., 2021).

559 In the interactions between RN and all metallic ions, there was an affinity with COO^- , C-O
560 and OH of phenolics. This characteristic also aligns with the previous characterization of samples,
561 indicating that RN presents higher humification and abundance of oxygenated groups than RC-I and

562 RC-II. This preference for interaction with COO^- is attributed to the higher quantity of such groups
563 in RN, as highlighted in previous studies (Constantino et al., 2021). This characteristic is further
564 supported by the ^{13}C NMR analysis, which suggests that RN samples have less hydrophobicity than
565 RC-I and RC-II.

566 The interaction between all samples and Fe (III) primarily involves COO^- . This
567 characteristic has been extensively studied in the literature, indicating that oxygenated groups play a
568 significant role in the interaction with Fe (III) based on the hard and soft acid–base (HSAB) rule
569 (Fujii et al., 2014; Stumm & Morgan, 2012). Fe (III) possesses incomplete d orbitals ($3d^5$),
570 exhibiting a hard acid characteristic (electron acceptor), while oxygenated groups (mainly COO^- , in
571 this case) exhibit hard basic characteristics (electron donor). Therefore, following the HSAB rule,
572 both have more suitable characteristics for interaction. Additionally, in a previous study conducted
573 in the same watershed, the majority of the metals, including Fe and Al, were quantified in the
574 particulate fraction ($> 0.45 \mu\text{m}$), indicating the possible interaction of these metals with dissolved
575 organic matter (Constantino et al., 2019).

576

577 **Conclusion**

578

579 The AHS from the dry season exhibited aromatic moieties and alkyl structures of
580 autochthonous origin. In contrast, AHS from the rainy season contained both aromatic and alkyl
581 moieties, but with an allochthonous source, including aromatic structures derived from lignin and
582 polysaccharides. The distinct molecular compositions clearly influenced the interaction capacities
583 with the tested metal ions. Structures with more aromatic moieties showed higher stability in
584 complex formation but lower complexation capacities. Conversely, those with more aliphatic
585 compounds exhibited higher complexation capacities but less stable complexes. The Complexation
586 Capacity (CC) of AHS helps predict the environmental behavior of metal species in the rivers of
587 this study area, the results indicate that during the rainy season, there is a higher potential for the

53

27

54

588 complexation of metals with natural organic matter, such as Cu (II), Al (III), and Fe (III), due to the
589 molecular characteristics that provide more oxygenated functional groups. In contrast, during the
590 dry season, AHS exhibits lower CC abilities, although the input of metals is also reduced due to
591 fewer rainy events. This suggests an ecological equilibrium where AHS can maintain metals in a
592 complex and unavailable state. However, any additional influx of metals resulting from
593 anthropogenic activities could disrupt this balance and lead to environmental deregulation.

594

595 **Acknowledgments**

596 Authors thank the student Giovanna P. Gama for the help in the aquatic humic substance
597 extraction and the Professor Maurício Boscolo for the support in the FTIR analysis.

598

599 **Funding**

600 This work was supported by a sponsor from Foundation for Research Support of the State of
601 São Paulo (FAPESP) grants 05/51242-8 and 15/22954-1 and National Council for Scientific and
602 Technological Development (CNPq) 303232/2022-6. L.R.B. acknowledges the scholarship from
603 FAPESP (grants 17/05575-2 and 17/17991-0).

604

605 **Author contribution**

606 Isabela Carreira Constantino contributed to the experimental design, execution of complexation
607 assays, formal analysis of the data, and original draft writing. Lucas Raimundo Bento contributed to
608 the formal analysis of NMR and Thermochemolysis, as well as the writing of the original draft.
609 Vinicius Sarracini Santos worked on the formal analysis of 2D-COS data and reviewed the
610 manuscript. Leila Soares da Silva contributed to the experimental design and execution of
611 complexation assays. Amanda Maria Tadini and Stéphane Mounier contributed to the formal
612 analysis of PARAFAC. Alessandro Piccolo and Riccardo Spaccini supported the analysis of
613 Thermochemolysis and NMR. Marinônio Lopes Cornélio participated in the formal analysis of 2D-
614 COS. Fabiana Maria Monteiro Paschoal and Ézio Sargentini Junior provided resources for sampling
615 and extraction of humic substances in the Amazon region. Altair Benedito Moreira and Márcia
616 Cristina Bisinoti participated in resource funding, investigation, and supervision of this manuscript.
617 All authors reviewed the manuscript.

618

619 **Data availability**

55

56

620 The datasets generated during and/or analyzed during the current study are available from the
621 corresponding author on reasonable request.

622

623 **Declarations**

624 **Ethical approval**

625 All authors have read, understood, and have complied as applicable with the statement on “Ethical
626 responsibilities of Authors” as found in the Instructions for Authors.

627

628 **Competing interests**

629 The authors declare that they have no competing interests.

630

631 **References**

- 632 Reasi, H. A., Wood, C. M., & Smith, D. S. (2011). Physicochemical and spectroscopic properties of
633 natural organic matter (NOM) from various sources and implications for ameliorative effects on
634 metal toxicity to aquatic biota. *Aquatic Toxicology*, *103*(3), 179–190.
635 <https://doi.org/10.1016/j.aquatox.2011.02.015>
- 636 Fontes, M. C. G., Pereira, C. C. C., & Esteves da Silva, J. C. G. (2007). MCR of the quenching of the
637 EEM of fluorescence of dissolved organic matter by metal ions. *Analytica Chimica Acta*, *595*(1-2
638 SPEC. ISS.), 9–18. <https://doi.org/10.1016/j.aca.2006.12.017>
- 639 Bento, L. R., Melo, C. A., Ferreira, O. P., Moreira, A. B., Mounier, S., Piccolo, A., Spaccini, R., &
640 Bisinoti, M. C. (2020). Humic extracts of hydrochar and Amazonian Dark Earth: Molecular
641 characteristics and effects on maize seed germination. *Science of the Total Environment*, *708*.
642 <https://doi.org/10.1016/j.scitotenv.2019.135000>
- 643 Bento, L. R., Spaccini, R., Cangemi, S., Mazzei, P., de Freitas, B. B., de Souza, A. E. O., Moreira, A. B.,
644 Ferreira, O. P., Piccolo, A., & Bisinoti, M. C. (2021). Hydrochar obtained with by-products from
645 the sugarcane industry: Molecular features and effects of extracts on maize seed germination.
646 *Journal of Environmental Management*, *281*. <https://doi.org/10.1016/j.jenvman.2020.111878>
- 647 Boguta, P., D’Orazio, V., Sokołowska, Z., & Senesi, N. (2016). Effects of selected chemical and
648 physicochemical properties of humic acids from peat soils on their interaction mechanisms with
649 copper ions at various pHs. *Journal of Geochemical Exploration*, *168*, 119–126.
650 <https://doi.org/10.1016/j.gexplo.2016.06.004>
- 651 Brailsford, F. L., Glanville, H. C., Golyshin, P. N., Johnes, P. J., Yates, C. A., & Jones, D. L. (2019).
652 Microbial uptake kinetics of dissolved organic carbon (DOC) compound groups from river water
653 and sediments. *Scientific Reports*, *9*(1), 11229. <https://doi.org/10.1038/s41598-019-47749-6>
- 654 BRASIL, Ministério do Planejamento e Orçamento/Fundação Instituto Brasileiro de Geografia e
655 Estatística. Portaria PR-470, de 28 de junho de 2023. Diário Oficial da União, nº122, de 29 de Junho
656 de 2023 (2023). [https://www.in.gov.br/web/dou/-/portaria-pr-470-de-28-de-junho-de-2023-
657 493169747](https://www.in.gov.br/web/dou/-/portaria-pr-470-de-28-de-junho-de-2023-493169747)
- 658 Barstea, E. M., Mounier, S., Redon, R., & Popa, C. L. (2020). Role of non-fluorescent chromophores in
659 inner filter effect correction and PARAFAC decomposition. *Spectrochimica Acta Part A:
660 Molecular and Biomolecular Spectroscopy*, *229*, 117878.
661 <https://doi.org/10.1016/j.saa.2019.117878>
- 662 Catalán, N., Obrador, B., Felip, M., & Pretus, J. L. (2013). Higher reactivity of allochthonous vs.
663 autochthonous DOC sources in a shallow lake. *Aquatic Sciences*, *75*(4), 581–593.
664 <https://doi.org/10.1007/s00027-013-0302-y>

57

58

29

665 Chen, W., Habibul, N., Liu, X. Y., Sheng, G. P., & Yu, H. Q. (2015). FTIR and synchronous
666 fluorescence heterospectral two-dimensional correlation analyses on the binding characteristics of
667 copper onto dissolved organic matter. *Environmental Science and Technology*, *49*, 2052–2058.
668 <https://doi.org/10.1021/es5049495>

669 Chen, W., Qian, C., Liu, X. Y., & Yu, H. Q. (2014). Two-dimensional correlation spectroscopic analysis
670 on the interaction between humic acids and TiO₂ nanoparticles. *Environmental Science and*
671 *Technology*, *48*(19), 11119–11126.
672 https://doi.org/10.1021/ES502502N/SUPPL_FILE/ES502502N_SI_001.PDF

673 Coble, P. G., Lead, J., Baker, A., Reynolds, D. M., & Spencer, R. G. (2014). *Aquatic Organic Matter*
674 *Fluorescence* (P. G. Coble, J. Lead, A. Baker, D. M. Reynolds, & R. G. Spencer, Eds.). Cambridge
675 University Press.

676 Coimbra Horbe, A. M., de Andrade Queiroz, M. M., Veloso Moura, C. A., & Galarza Toro, M. A.
677 (2013). Geoquímica das águas do médio e baixo rio Madeira e seus principais tributários -
678 Amazonas -Brasil. *Acta Amazonica*, *43*(4), 489–504. [https://doi.org/10.1590/S0044-](https://doi.org/10.1590/S0044-59672013000400011)
679 [59672013000400011](https://doi.org/10.1590/S0044-59672013000400011)

680 Constantino, I. C., Teodoro, G. C., Moreira, A. B., Paschoal, F. M. M., Trindade, W. G., & Bisinoti, M.
681 C. (2019). Distribution of metals in the waters and sediments of rivers in central amazon region,
682 Brazil. *Journal of the Brazilian Chemical Society*, *30*(9), 1906–1915.
683 <https://doi.org/10.21577/0103-5053.20190100>

684 Constantino, I. C., Viana, J. G., Teixeira, P. A., Moreira, A. B., Gama, G. P., Paschoal, F. M. M.,
685 Sargentini, É., & Bisinoti, M. C. (2021). Interaction of Pb, Ni and Cd with aquatic humic
686 substances of amazonian blackwater rivers. *Journal of the Brazilian Chemical Society*, *32*(2), 260–
687 268. <https://doi.org/10.21577/0103-5053.20200176>

688 de Mastro, F., Coccozza, C., Traversa, A., Savy, D., Abdelrahman, H. M., & Brunetti, G. (2019).
689 Influence of crop rotation, tillage and fertilization on chemical and spectroscopic characteristics of
690 humic acids. *Plos One*, *14*(6), 1–15. <https://doi.org/10.1371/journal.pone.0219099>

691 de Moraes, C. P., Tadini, A. M., Bento, L. R., Oursel, B., Guimaraes, F. E. G., Martin-Neto, L., Mounier,
692 S., & Milori, D. M. B. P. (2021). Assessing extracted organic matter quality from river sediments
693 by elemental and molecular characterization: Application to the Tietê and Piracicaba Rivers (São
694 Paulo, Brazil). *Applied Geochemistry*, *131*(July). <https://doi.org/10.1016/j.apgeochem.2021.105049>

695 Signac, M. F., Knicker, H., & Kogel-Knabner, I. (2003). Effect of N content and soil texture on the
696 decomposition of organic matter in forest soils as revealed by solid-state CPMAS NMR
697 spectroscopy. *Abstracts of Papers of the American Chemical Society*, *33*(12), 1715–1726.

698 Rosos, M., Nebbioso, A., & Piccolo, A. (2018). Humeomics: A key to unravel the humic pentagram.
699 *Applied Soil Ecology*, *123*(July 2017), 513–516. <https://doi.org/10.1016/j.apsoil.2017.07.027>

700 Jiji, M., Imaoka, A., Yoshimura, C., & Waite, T. D. (2014). Effects of molecular composition of
701 natural organic matter on ferric iron complexation at circumneutral pH. *Environmental Science and*
702 *Technology*, *48*(8), 4414–4424.
703 https://doi.org/10.1021/ES405496B/SUPPL_FILE/ES405496B_SI_001.PDF

704 Unkey, C. P., Conley, D. J., & Stedmon, C. A. (2019). Sediment alkaline-extracted organic matter
705 (AEOM) fluorescence: An archive of Holocene marine organic matter origins. *Science of the Total*
706 *Environment*, *676*, 298–304. <https://doi.org/10.1016/j.scitotenv.2019.04.170>

707 Garnier, C., Pižeta, I., Mounier, S., Benaïm, J. Y., & Branica, M. (2004). Influence of the type of
708 titration and of data treatment methods on metal complexing parameters determination of single and
709 multi-ligand systems measured by stripping voltammetry. *Analytica Chimica Acta*, *505*(2), 263–
710 275. <https://doi.org/10.1016/j.aca.2003.10.066>

711 Huang, M., Li, Z., Huang, B., Luo, N., Zhang, Q., Zhai, X., & Zeng, G. (2018). Investigating binding
712 characteristics of cadmium and copper to DOM derived from compost and rice straw using EEM-
713 PARAFAC combined with two-dimensional FTIR correlation analyses. *Journal of Hazardous*
714 *Materials*, *344*, 539–548. <https://doi.org/10.1016/j.jhazmat.2017.10.022>

715 Jardim, W. F., Bisinoti, M. C., Fadini, P. S., & da Silva, G. S. (2010). Mercury redox chemistry in the
716 Negro River basin, Amazon: The role of organic matter and solar light. *Aquatic Geochemistry*,
717 16(2), 267–278. <https://doi.org/10.1007/s10498-009-9086-z>

718 Ank, W. J., Wittmann, F., Schöngart, J., & Piedade, M. T. F. (2015). A classification of the major
719 habitats of Amazonian black-water river floodplains and a comparison with their white-water
720 counterparts. *Wetlands Ecology and Management*, 23(4), 677–693. [https://doi.org/10.1007/s11273-](https://doi.org/10.1007/s11273-721)
721 015-9412-8

722 Rögel-Knabner, I. (1997). ¹³C and ¹⁵N NMR spectroscopy as a tool in soil organic matter studies.
723 *Geoderma*, 80(3–4), 243–270. [https://doi.org/10.1016/S0016-7061\(97\)00055-4](https://doi.org/10.1016/S0016-7061(97)00055-4)

724 Ungolos, A., Samaras, P., Tsiridis, V., Petala, M., & Sakellaropoulos, G. (2006). Bioavailability and
725 Toxicity of Heavy Metals in the Presence of Natural Organic Matter. *Journal of Environmental*
726 *Science and Health, Part A*, 41(8), 1509–1517. <https://doi.org/10.1080/10934520600754706>

727 Lee, Y. K., Hong, S., & Hur, J. (2021). Copper-binding properties of microplastic-derived dissolved
728 organic matter revealed by fluorescence spectroscopy and two-dimensional correlation
729 spectroscopy. *Water Research*, 190, 116775.
730 <https://doi.org/https://doi.org/10.1016/j.watres.2020.116775>

731 Lee, Y. P., Wong, K. H., Obata, H., Nishitani, K., Ogawa, H., Fukuda, H., & Lu, C. J. (2023).
732 Distributions of humic substances in an estuarine region (Otsuchi Bay, Japan) determined using
733 electrochemical and optical methods. *Marine Chemistry*, 256.
734 <https://doi.org/10.1016/j.marchem.2023.104301>

735 Eenheer, J. A., & Croué, J.-P. (2003). Characterizing Dissolved Aquatic Matter. *Environmental Science*
736 *and Technology*, 37, 18A-26A.

737 Li, W., Zhang, F., Ye, Q., Wu, D., Wang, L., Yu, Y., Deng, B., & Du, J. (2017). Composition and
738 copper binding properties of aquatic fulvic acids in eutrophic Taihu Lake, China. *Chemosphere*,
739 172, 496–504. <https://doi.org/10.1016/J.CHEMOSPHERE.2017.01.008>

740 Luciani, X., Mounier, S., Redon, R., & Bois, A. (2009). A simple correction method of inner filter
741 effects affecting FEEM and its application to the PARAFAC decomposition. *Chemometrics and*
742 *Intelligent Laboratory Systems*, 96(2), 227–238.
743 <https://doi.org/https://doi.org/10.1016/j.chemolab.2009.02.008>

744 Luo, H., Cheng, Q., He, D., Wang, X., & Pan, X. (2022). Effects of photo-irradiation on mercury
745 binding to dissolved organic matter: Insights from FT-IR and synchronous fluorescence two-
746 dimensional correlation spectroscopy. *Chemosphere*, 287, 132027.
747 <https://doi.org/10.1016/J.CHEMOSPHERE.2021.132027>

748 Maurice, P. A., Pullin, M. J., Cabaniss, S. E., Zhou, Q., Namjesnik-Dejanovic, K., & Aiken, G. R.
749 (2002). A comparison of surface water natural organic matter in raw filtered water samples, XAD,
750 and reverse osmosis isolates. *Water Research*, 36(9), 2357–2371.
751 [https://doi.org/https://doi.org/10.1016/S0043-1354\(01\)00442-0](https://doi.org/https://doi.org/10.1016/S0043-1354(01)00442-0)

752 Melo, C. A., De Toffoli, A. L., Moreira, A. B., & Bisinoti, M. C. (2012). Solar radiation effect on the
753 complexation capacity of aquatic humic substances with metals. *Journal of the Brazilian Chemical*
754 *Society*, 23(10), 1871–1879. <https://doi.org/10.1590/S0103-50532012005000059>

755 Mounier, S., Zhao, H., Garnier, C., & Redon, R. (2011). Copper complexing properties of dissolved
756 organic matter: PARAFAC treatment of fluorescence quenching. *Biogeochemistry*, 106(1), 107–
757 116. <https://doi.org/10.1007/s10533-010-9486-6>

758 Muller, F. L. L., Tankéré-Muller, S. P. C., & Tang, C. H. (2024). Terrigenous humic substances regulate
759 the concentrations of dissolved Fe and Cu (but not Al, Mn, Ni or Zn) in the Gaoping River plume.
760 *Science of the Total Environment*, 906. <https://doi.org/10.1016/j.scitotenv.2023.167374>

761 Lebbioso, A., & Piccolo, A. (2009). Molecular rigidity and diffusivity of Al³⁺ And Ca²⁺ humates as
762 revealed by NMR spectroscopy. *Environmental Science and Technology*, 43, 2417–2424.
763 <https://doi.org/10.1021/es802807y>

- 764ebbioso, A., & Piccolo, A. (2011). Basis of a humeomics science: Chemical fractionation and
765 molecular characterization of humic biosuprastructures. *Biomacromolecules*, 12(4), 1187–1199.
766 <https://doi.org/10.1021/bm101488e>
- 767ebbioso, A., & Piccolo, A. (2012). Advances in humeomics: Enhanced structural identification of
768 humic molecules after size fractionation of a soil humic acid. *Analytica Chimica Acta*, 720, 77–90.
769 <https://doi.org/10.1016/j.aca.2012.01.027>
- 770ebbioso, A., & Piccolo, A. (2013). Molecular characterization of dissolved organic matter (DOM): a
771 critical review. *Analytical and Bioanalytical Chemistry*, 37(405), 109–124.
772 <https://doi.org/10.1007/s00216-012-6363-2>
- 773oda, I., & Ozaki, Y. (2004). Two-Dimensional Correlation Spectroscopy - Applications in Vibrational
774 and Optical Spectroscopy. In *Two-Dimensional Correlation Spectroscopy - Applications in*
775 *Vibrational and Optical Spectroscopy*. John Wiley & Sons, Inc.
- 776liveira, L. C. De, Jr, É. S., Rosa, A. H., Rocha, J. C., Simões, M. L., Martin-neto, L., Silva, W. T. L., &
777 Serudo, R. L. (2007). *The influence of seasonless on the structural characteristics of aquatic*
778 *humic substances extracted from Negro River (Amazon State) waters : Interactions with Hg (II)*.
779 18(4), 860–868.
- 780avia, D. L., Lampman, G. M., & Kriz, G. S. (2008). Introduction to Spectroscopy. In *Thomson*
781 *Learning, Inc*.
- 782ccolo, A. (2002). The supramolecular structure of humic substances: A novel understanding of humus
783 chemistry and implications in soil science. *Advances in Agronomy*, 75(December 2002), 57–134.
784 [https://doi.org/10.1016/S0065-2113\(02\)75003-7](https://doi.org/10.1016/S0065-2113(02)75003-7)
- 785edon, R., & Mounier, S. (2018). *ProgMEEF*. <https://woms18.univ-tln.fr/progmeef/>
- 786omão, L. P. C., Castro, G. R., Rosa, A. H., Rocha, J. C., Padilha, P. M., & Silva, H. C. (2003).
787 Tangential-flow Ultrafiltration: A versatile methodology for determination of complexation
788 parameters in refractory organic matter from Brazilian water and soil samples. *Analytical and*
789 *Bioanalytical Chemistry*, 375(8), 1097–1100. <https://doi.org/10.1007/s00216-002-1728-6>
- 790osa, J. M. de la, Faria, S. R., Varela, M. E., Knicker, H., Gonzalez-vila, F. javier, Gonzales-perez, jose
791 antonio, & Keizer, J. (2012). Characterization of wildfire effects on soil organic matter using
792 analytical pyrolysis. *Geoderma*, 191, 24–30. <https://doi.org/10.1016/j.geoderma.2012.01.032>
- 793yan, D. K., & Weber, J. H. (1982). Fluorescence Quenching Titration for Determination of Complexing
794 Capacities and Stability Constants of Fulvic Acid. *Analytical Chemistry*, 54(6), 986–990.
795 <https://doi.org/10.1021/ac00243a033>
- 796antos, V. S., Moura, B. R., Constantino, I. C., Metzker, G., Boscolo, M., Cornélio, M. L., Ferreira, O.
797 P., Mounier, J. L. S., Hajjoul, H., Bisinoti, M. C., Junior, F. H. S., & Moreira, A. B. (2021).
798 Chelating properties of humic-like substances obtained from process water of hydrothermal
799 carbonization. *Environmental Technology and Innovation*, 23, 101688.
800 <https://doi.org/10.1016/j.eti.2021.101688>
- 801enesi, N., Miano, T. M., Provenzano, M. R., & Brunetti, G. (1991). Characterization, Diferentation and
802 Classification of Humic Substances by Fluorescencia Spectroscopy. *Soil Science*, 152(4), 259–271.
- 803bares da Silva, L., Constantino, I. C., Bento, L. R., Tadini, A. M., Bisinoti, M. C., Boscolo, M.,
804 Ferreira, O. P., Mounier, S., Piccolo, A., Spaccini, R., Cornélio, M. L., & Moreira, A. B. (2020).
805 Humic extracts from hydrochar and Amazonian Anthrosol: Molecular features and metal binding
806 properties using EEM-PARAFAC and 2D FTIR correlation analyses. *Chemosphere*, 256.
807 <https://doi.org/10.1016/j.chemosphere.2020.127110>
- 808paccini, R., Cozzolino, V., Di Meo, V., Savy, D., Drosos, M., & Piccolo, A. (2019). Bioactivity of
809 humic substances and water extracts from compost made by ligno-cellulose wastes from
810 biorefinery. *Science of the Total Environment*, 646, 792–800.
811 <https://doi.org/10.1016/j.scitotenv.2018.07.334>
- 812umm, W., & Morgan, J. J. (2012). *Aquatic chemistry: chemical equilibria and rates in natural waters*.
813 John Wiley & Sons.

814 Radini, A. M., Campanha, M. B., Moreira, A. B., & Bisinoti, M. C. (2013). Copper(II) and nickel (II)
815 complexation capacity of dissolved organic matter from rivers of agricultural and urban areas in the
816 state of São Paulo. *Journal of the Brazilian Chemical Society*, 24(11), 1789–1797.
817 <https://doi.org/10.5935/0103-5053.20130224>

818 Radini, A. M., Constantino, I. C., Nuzzo, A., Spaccini, R., Piccolo, A., Moreira, A. B., & Bisinoti, M. C.
819 (2015). Characterization of typical aquatic humic substances in areas of sugarcane cultivation in
820 Brazil using tetramethylammonium hydroxide thermochemolysis. *Science of the Total
821 Environment*, 518–519, 201–208. <https://doi.org/10.1016/j.scitotenv.2015.02.103>

822 Radini, A. M., Mounier, S., & Milori, D. M. B. P. (2020). Modeling the quenching of fluorescence from
823 organic matter in Amazonian soils. *Science of the Total Environment*, 698.
824 <https://doi.org/10.1016/j.scitotenv.2019.134067>

825 Radini, A. M., Nicolodelli, G., Marangoni, B. S., Mounier, S., Montes, C. R., & Milori, D. M. B. P.
826 (2019). Evaluation of the roles of metals and humic fractions in the podzolization of soils from the
827 Amazon region using two analytical spectroscopy techniques. *Microchemical Journal*, 144(October
828 2018), 454–460. <https://doi.org/10.1016/j.microc.2018.10.009>

829 Hurman, E. M., & Malcolm, R. L. (1981). Preparative isolation of aquatic humic substances.
830 *Environmental Science & Technology*, 15(4), 463–466. <https://doi.org/10.1021/es00086a012>

831 Traversa, A., D’Orazio, V., Mezzapesa, G. N., Bonifacio, E., Farrag, K., Senesi, N., & Brunetti, G.
832 (2014). Chemical and spectroscopic characteristics of humic acids and dissolved organic matter
833 along two Alfisol profiles. *Chemosphere*, 111, 184–194.
834 <https://doi.org/10.1016/j.chemosphere.2014.03.063>

835 Yguner-Demirel, C. S., & Bekbolet, M. (2011). Significance of analytical parameters for the
836 understanding of natural organic matter in relation to photocatalytic oxidation. *Chemosphere*, 84(8),
837 1009–1031. <https://doi.org/10.1016/j.chemosphere.2011.05.003>

838 Herrillo, M., Salzano, M., Cozzolino, V., Spaccini, R., & Piccolo, A. (2021). Bioactivity and
839 antimicrobial properties of chemically characterized compost teas from different green composts.
840 *Waste Management*, 120, 98–107. <https://doi.org/10.1016/j.wasman.2020.11.013>

841 Westerhoff, P., Mezyk, S. P., Cooper, W. J., & Minakata, D. (2007). Electron pulse radiolysis
842 determination of hydroxyl radical rate constants with Suwannee river fulvic acid and other
843 dissolved organic matter isolates. *Environmental Science and Technology*, 41(13), 4640–4646.
844 <https://doi.org/10.1021/es062529n>

845 Tang, F., Tang, C., & Antonietti, M. (2021). Natural and artificial humic substances to manage minerals,
846 ions, water, and soil microorganisms. *Chemical Society Reviews*, 50(10), 6221–6239.
847 <https://doi.org/10.1039/D0CS01363C>

848 Guan, Y., Cai, X., Tan, B., Zhou, S., & Xing, B. (2018). Molecular insights into reversible redox sites in
849 solid-phase humic substances as examined by electrochemical in situ FTIR and two-dimensional
850 correlation spectroscopy. *Chemical Geology*, 494, 136–143.
851 <https://doi.org/10.1016/J.CHEMGEO.2018.07.029>

852 Zepp, R. G., Sheldon, W. M., & Moran, M. A. (2004). Dissolved organic fluorophores in southeastern
853 US coastal waters: correction method for eliminating Rayleigh and Raman scattering peaks in
854 excitation–emission matrices. *Marine Chemistry*, 89(1), 15–36.
855 <https://doi.org/https://doi.org/10.1016/j.marchem.2004.02.006>
856